Liquid Crystals
Publication details, including instructions for authors and subscription information:
http://www.informaworld.com/smpp/title~content=t713926090

Computational study of the texture formation in mesophase pitch-based carbon fibres

Shujuan Hong[a]; Philip K. Chan[a]
[a] Department of Chemical Engineering, Ryerson University, Toronto, Ontario M5B 2K3, Canada

To cite this Article Hong, Shujuan and Chan, Philip K.(2006) 'Computational study of the texture formation in mesophase pitch-based carbon fibres', Liquid Crystals, 33: 3, 295 — 306
To link to this Article: DOI: 10.1080/02678290500242213
URL: http://dx.doi.org/10.1080/02678290500242213

Liquid Crystals, Vol. 33, No. 3, March 2006, 295–306

Taylor & Francis
Taylor & Francis Group

Computational study of the texture formation in mesophase pitch-based carbon fibres

SHUJUAN HONG and PHILIP K. CHAN*

Department of Chemical Engineering, Ryerson University, 350 Victoria Street, Toronto, Ontario M5B 2K3, Canada

(*Received 27 January 2005; in final form 10 May 2005; accepted 12 May 2005*)

This paper studies the thermal relaxation phenomena after melt-extrusion of a rigid discotic uniaxial nematic mesophase pitch using mathematical modelling and computer simulation. The Ericksen and Landau–de Gennes continuum theories are used to investigate the structure development and texture formation across mesophase pitch-based carbon fibres. The two-dimensional model captures five types of transverse patterns, which match the commonly observed textures for mesophase pitch-based carbon fibres. They are: random, zig-zagged radial, radial, quasi-onion and onion. These textures represent the various combinations possible from the interplay between structure (i.e. texture) development and cooling during the fibre spinning process. During the thermal relaxation after the cessation of extensional flow the discotic nematic molecules store elastic free energy decays. The distorted nematic molecular profiles reorient to release the stored elastic free energy. The difference in time scales for molecular reorientation and thermal relaxation result in different transverse textures. The rate at which the fibres are cooled is the main factor in controlling the structure development. A slow cooling rate would permit the nematic discotic molecules to reorient to a well-developed (radial or onion) texture. The random texture is a result of rapid quenching. The numerical results are consistent with published experimental observations.

1. Introduction

High performance mesophase pitch-based carbon fibres are made from liquid crystalline materials composed of nematic discotic molecules. These molecules can be aligned in certain directions to form well defined structures [1–7]. It is these well-defined structures that give these materials excellent mechanical and transport properties, and provide carbon fibres with wide applications ranging from the aerospace industry to sporting goods [5–10]. The transport properties, transverse structure development, and texture formation have been the subject of numerous experimental and theoretical studies. Previous work [9–14] has indicated that a well-defined structure is created during the melt spinning process. Spinning parameters such as melt spinning temperature, melt viscosity, and spinneret structure all affect the texture formation in carbon fibres [6, 8, 14].

Successful manufacturing of high performance carbon fibres from mesophase pitch depends on the control of texture formation, i.e. molecular orientation. The different orientations of the discotic molecules give rise to various cross-sectional textures. The most commonly observed are the radial, onion and random textures [1–3]. Mesophase carbonaceous fibres with random textures tend to exhibit higher tensile and compressive properties. By contrast, fibres with radial transverse textures have superior transport properties, such as thermal conductivity [8, 15]. Although substantial progress has been made during the past four decades, the structure development and texture formation for carbon fibres are still not completely understood.

Theoretical studies using available liquid crystal continuum theories to model and simulate the structure development and texture formation have been performed by Edie *et al.* [6, 14] and Rey *et al.* [16–23]. Nematic discotic liquid crystal molecules tend to align their short axis along a common direction, defined by a unit vector called the director **n**. The degree of alignment along the director is defined as the scalar order parameter S [24–29]. Edie *et al.* [6, 14] modelled mesophase pitch molecules as rigid discotic nematics and studied their molecular orientation during fully developed channel flow. Their numerical results were consistent with pitch observed under a polarizing optical microscope. Singh and Rey [16–18] examined continuum theories such as the Leslie–Ericksen theory

*Corresponding author. Email: p4chan@ryerson.ca

Liquid Crystals
ISSN 0267-8292 print/ISSN 1366-5855 online © 2006 Taylor & Francis
http://www.tandf.co.uk/journals
DOI: 10.1080/02678290500242213

developed for nematic liquid crystals, and proposed that the theories can be extended to low molecular mass disc-like liquid crystal molecules to describe the flow behaviour of mesophase pitch. Wang and Rey [30] approximated the melt pitch to be a nematic discotic liquid crystal and assumed the melt spinning process to be an isothermal, incompressible, uniaxial, extensional flow. They modelled the dynamic behaviour of nematic discotic liquid crystal molecules using the Leslie–Ericksen and Frank elastic free energy theories and assumed a homogeneous order parameter S. Their simulation results concluded that: (1) minimizing the Frank elastic free energy is the mechanism of mode selection between the radial and onion textures, and (2) the onion (radial) texture forms at high or low temperatures, while a random texture is created in an intermediate temperature range. White and Buechler [31], however, suggested that the radial texture is formed at low viscosity and slow cooling, while the random texture would form at high viscosity and rapid quenching. Intermediate textures result from partial annihilation of disclinations.

Melt spinning is a complex non-isothermal process involving uniaxial flow, cooling and solidification. After leaving the spinneret, the melt pitch is cooled and solidified to form a fibre. This thermal relaxation involves heat transfer from the melt pitch to the cooling medium, which creates a radial temperature gradient across the fibre. Moreover, it is also during this thermal relaxation that the flow-induced structure starts to relax from a stressed high energy to a low energy state with a well defined structure. Since the material properties of carbon fibres depend on the molecular structure, it is crucial to understand the time evolution of the director and order parameter during the thermal relaxation period. A survey of the literature shows that this understanding is far from complete. The aim of this paper is to investigate numerically the structure development and texture formation during the thermal relaxation after cessation of uniaxial shear flow for carbonaceous mesophase pitch. We use the Ericksen [32] continuum theory incorporating the Landau–de Gennes free energy density [25]. This combination of liquid crystalline theory has already been used successfully by Chan and Rey [33] to study the banded texture formation in liquid crystalline polymers after cessation of shear flow.

The objectives of this paper are: (1) to present results from a numerical study on the thermal relaxation phenomena after steady extensional flow for a model incompressible uniaxial nematic pitch phase composed of rigid disc-like molecules using the Ericksen and Landau–de Gennes nematic continuum theories, (2) to characterize the structure development and texture formation during thermal relaxation after cessation of extensional flow and (3) to examine the effects of mesophase pitch material properties and process conditions on the texture formation and evolution. The next section outlines the Ericksen and Landau–de Gennes continuum theories and details the development of the governing equations. The results are presented and discussed in § 3 and the conclusions are given in § 4.

2. Continuum theories and problem formulation

In Cartesian tensorial notation for an incompressible fluid, the linear momentum balance equation is

$$\rho \dot{\mathbf{V}} = \mathbf{F} + \nabla \cdot \boldsymbol{\tau}. \tag{1}$$

The constitutive equation for the stress tensor $\boldsymbol{\tau}$, according to the Ericksen theory [32], is given as

$$\begin{aligned} \boldsymbol{\tau} = & -p\boldsymbol{\delta} - \frac{\partial f_{\mathrm{L}}}{\partial \nabla \mathbf{n}} \cdot (\nabla \mathbf{n})^{\mathrm{T}} - \frac{\partial f_{\mathrm{L}}}{\partial \nabla S} \nabla S \\ & + \beta_1^S(S)\dot{S}\,\mathbf{nn} + \alpha_1^S(S)(\mathbf{nn} : \mathbf{A})\mathbf{nn} \\ & + \alpha_2^S(S)\mathbf{nN} + \alpha_3^S(S)\mathbf{Nn} + \alpha_4^S(S)\mathbf{A} \\ & + \alpha_5^S(S)\mathbf{nn}\cdot\mathbf{A} + \alpha_6^S(S)\mathbf{A}\cdot\mathbf{nn}, \end{aligned} \tag{2}$$

where the kinematic quantities are defined as follows:

$$\mathbf{A} = \frac{1}{2}\left[(\nabla \mathbf{V})^{\mathrm{T}} + \nabla \mathbf{V}\right] \tag{3 a}$$

$$\mathbf{N} = \dot{\mathbf{n}} - \boldsymbol{\Omega}\cdot\mathbf{n} \tag{3 b}$$

$$\boldsymbol{\Omega} = \frac{1}{2}\left[(\nabla \mathbf{V})^{\mathrm{T}} - \nabla \mathbf{V}\right]. \tag{3 c}$$

In the above equations, ρ is the fluid density, $\mathbf{V}$ is the velocity, and $\mathbf{F}$ is the external body force per unit volume. The superimposed dot denotes the material time derivative. The Leslie viscosity coefficients $\{\alpha_i^S\}$, $i = 1, \ldots, 6$, and β_1^S all depend on S; p is the pressure, and $\boldsymbol{\delta}$ is the unit tensor. In addition, $\mathbf{N}$ is the angular velocity of the director relative to that of the fluid, $\mathbf{A}$ is the rate of deformation tensor, and $\boldsymbol{\Omega}$ is the vorticity tensor. The ijth Cartesian component of $\nabla\mathbf{n}$ and $\nabla\mathbf{V}$ are $\partial n_j/\partial x_i$ and $\partial V_j/\partial x_i$, respectively.

The Landau–de Gennes free energy density of the nematic material is defined as follows [25]:

$$f_L = f_o(T) + \frac{3}{4}A\left(T - T_{NI}^{+}\right)S^2 + \frac{1}{4}BS^3 + \frac{9}{16}CS^4 + \frac{3}{4}\left(L_1 + \frac{1}{6}L_2\right)(\nabla S)^2 + \frac{3}{8}L_2(\mathbf{n}\cdot\nabla S)^2 + \frac{9}{4}S^2\left[\left(L_1 + \frac{1}{2}L_2\right)(\nabla\cdot\mathbf{n})^2 + L_1(\mathbf{n}\cdot\nabla\times\mathbf{n})^2 + \left(L_1 + \frac{1}{2}L_2\right)(\mathbf{n}\times\nabla\times\mathbf{n})^2\right] + \frac{3}{2}L_2S(\nabla\cdot\mathbf{n})\times(\mathbf{n}\cdot\nabla S) + \frac{3}{4}L_2S(\mathbf{n}\times\nabla\times\mathbf{n})\cdot\nabla S \quad (4)$$

where f_o (T) is the isotropic free energy density at temperature T, and A, B, C, L_1, L_2 are material constants. T_{NI}^{+} is a temperature slightly below the clearing temperature T_{NI}, where the first order nematic–isotropic phase transition occurs. In this paper, we assume $T_{NI}^{+} = T_{NI}$ for simplicity. Equation (4) contains four groups of terms. The first four terms contain only the scalar order parameter. The next two terms account for the spatial variations in S. The following three terms account for director spatial variation, and is expanded as such to resemble the Frank–Oseen–Zocher free energy density, which is expressed as [24, 27]:

$$f_d = \frac{1}{2}\left[K_1(\nabla\cdot\mathbf{n})^2 + K_2(\mathbf{n}\cdot\nabla\times\mathbf{n})^2 + K_3(\mathbf{n}\times\nabla\times\mathbf{n})^2\right]. \quad (5)$$

It should be noted that, to second order in the Landau–de Gennes expression, there are only two independent elastic constants, whereas there are three independent Frank elastic constants, i.e. K_1 (for splay), K_2 (for twist) and K_3 (for bend) in the Frank–Oseen–Zocher free energy density. For rod-like nematic liquid crystals, K_3 is larger than K_1 and K_2, while for disc-like nematic liquid crystals K_2 is larger than K_1 and K_3. While the Frank elastic constants decrease quickly with increasing temperature, the Landau–de Gennes elastic coefficients L_1 and L_2 are independent of temperature. The relationships between the Landau elastic coefficients and the Frank elastic constants are as follows [34]:

$$L_1 = \frac{K_2}{2S^2} \quad (6\,a)$$

$$L_2 = \frac{K - K_2}{2S^2} \quad (6\,b)$$

$$K = K_1 = K_3. \quad (6\,c)$$

The last two terms in equation (4) represent the interaction between S and $\mathbf{n}$ and their spatial gradients. In this paper these four groups of terms are conveniently called the molecular free energy density f_S, the molecular elastic free energy density f_e, the Frank elastic free energy density f_d, and the coupling elastic free energy density f_C, respectively [33]. The coefficients A, B, and C are not known for a nematic discotic liquid crystal. It is then convenient to replace the terms introduced by these coefficients in the free energy density by the following Doi expression [35]:

$$f_S = k_B\upsilon T\left[\frac{1}{2}\left(1 - \frac{1}{3}U\right)S^2 - \frac{1}{9}US^3 + \frac{1}{6}US^4\right] \quad (7)$$

where k_B is the Boltzmann constant, υ is the disc concentration, and U is the dimensionless nematic potential expressed as:

$$U = \frac{3T_{NI}}{T}. \quad (8)$$

In equation (8), T_{NI} is the nematic–isotropic transition temperature, and T is the absolute temperature of the fibre. Since heat loss from the carbon fibre exiting the spinneret is through the surface and the fibre diameter is on the micron scale, it is plausible to assume that the dominant heat conduction direction is along the radial direction of the fibre. This means that it is also plausible to assume an effective thermal conductivity k_{th} for the mesophase carbonaceous fibre and to use the following form for the energy balance for heat conduction [36]:

$$\rho C_p\frac{\partial T}{\partial t} = k_{th}\nabla^2 T \quad (9)$$

where C_p is the heat capacity of the nematic phase at constant pressure per unit mass, and ρ is the nematic phase density.

According to the Ericksen [32] continuum theory, the balance equations for $\mathbf{n}$ and S are defined, respectively, as follows:

$$\dot{\mathbf{n}} = \Omega\cdot\mathbf{n} + \frac{\gamma_2^S(S)}{\gamma_1^S(S)}\left[\mathbf{n}\left(\mathbf{n}^T\cdot\mathbf{A}\cdot\mathbf{n}\right) - \mathbf{A}\cdot\mathbf{n}\right] - \frac{1}{\gamma_1^S(S)}\frac{\delta f_L}{\delta\mathbf{n}} \quad (10\,a)$$

$$\dot{S} = -\frac{1}{\beta_2^S(S)}\frac{\delta f_L}{\delta S} - \frac{\beta_1^S(S)}{\beta_2^S(S)}\mathbf{n}^T\cdot\mathbf{A}\cdot\mathbf{n} \quad (10\,b)$$

where γ_1^S, γ_2^S and β_1^S, β_2^S are viscosity coefficients that depend on S. In addition,

$$\gamma_1 = \alpha_3 - \alpha_2 \quad (11\,a)$$

$$\gamma_2 = \alpha_6 - \alpha_5 = \alpha_3 + \alpha_2. \quad (11\,b)$$

The equality in equation (11 b) is due to Parodi [37]; therefore, there are only five independent Leslie viscosity coefficients for nematic liquid crystal flow. In

the Ericksen continuum theory all α_i^S vary with the scalar order parameter S; these relationships are listed in the Appendix. $\delta f_L/\delta(*)$ denotes the functional derivative of f_L with respect to (*).

The rest of this section consists of the development of the partial differential equations that govern the time evolution of the temperature, the director, and the scalar order parameter within the carbonaceous mesophase fibre during the cooling process after it is pulled out of the spinneret. Figure 1 shows the schematic representation of the disc-like molecules within a section of a carbonaceous mesophase fibre of radius R, and the definition of the coordinate systems. The polar coordinate r–ϕ is expressed with dashed lines. The cartesian coordinate x–y is expressed with solid lines. θ is the planar director orientation angle measured in radians, which is the angle between director **n** and polar r at point (x, y).

We assume in this two-dimensional study: (1) the inertia of the director is negligible and neglected, (2) there is no external force **F**, (3) the director remains within the xy-plane, and (4) backflows are negligible and neglected. The director field is defined as

$$\mathbf{n} = (\cos\theta,\ \sin\theta,\ 0) \tag{12}$$

where the unit length constraint, $\mathbf{n}\cdot\mathbf{n}=1$, is automatically satisfied. Within this planar two-dimensional approximation, the three unknowns are as follows:

$$T = T(x, y, t),\ \theta = \theta(x, y, t),\ S = S(x, y, t). \tag{13 a,b,c}$$

The three equations that govern the behaviour of temperature T, director orientation θ, and the scalar order parameter S are the energy balance equation of the system [see equation (9)], the z-component of the angular momentum balance [see equation (10 a)], and the scalar orientational order balance [see equation (10 b)]. They are, respectively:

$$\rho C_p \frac{\partial T}{\partial t} = k_{th}\left(\frac{\partial^2 T}{\partial x^2} + \frac{\partial^2 T}{\partial y^2}\right) \tag{14 a}$$

$$\begin{aligned} -\gamma_1 \frac{\partial \theta}{\partial t} = {} & \kappa_1\left(\frac{\partial\theta}{\partial x} + \frac{\partial\theta}{\partial y}\right)\left(\frac{\partial S}{\partial x} + \frac{\partial S}{\partial y}\right) + \kappa_2\left(\frac{\partial^2\theta}{\partial x^2} + \frac{\partial^2\theta}{\partial y^2}\right) \\ & + \kappa_3 \frac{\partial S}{\partial x}\frac{\partial S}{\partial y} + \kappa_4\left(\frac{\partial S}{\partial x}\right)^2 + \kappa_5\left(\frac{\partial S}{\partial y}\right)^2 \\ & + \kappa_6 \frac{\partial^2 S}{\partial x^2} + \kappa_7 \frac{\partial^2 S}{\partial y^2} + \kappa_8\left(\frac{\partial\theta}{\partial x} - \frac{\partial\theta}{\partial y}\right)\left(\frac{\partial S}{\partial x} - \frac{\partial S}{\partial y}\right) \end{aligned} \tag{14 b}$$

$$\begin{aligned} -\gamma_1 \frac{\partial S}{\partial t} = {} & k_B \upsilon T\left[\left(1 - \frac{T_{NI}}{T}\right)S - \frac{T_{NI}}{T}S^2 + 2\frac{T_{NI}}{T}S^3\right](3 + 6S^2) \\ & + \kappa_9\left[\left(\frac{\partial\theta}{\partial x}\right)^2 + \left(\frac{\partial\theta}{\partial y}\right)^2\right] + \kappa_{10}\left(\frac{\partial^2 S}{\partial x^2} + \frac{\partial^2 S}{\partial y^2}\right) \\ & + \kappa_{11}\frac{\partial\theta}{\partial x}\frac{\partial S}{\partial x} + \kappa_{12}\frac{\partial\theta}{\partial y}\frac{\partial S}{\partial y} + \kappa_{13}\frac{\partial^2 S}{\partial x^2} + \kappa_{14}\frac{\partial^2 S}{\partial y^2} \\ & + \kappa_{15}\frac{\partial^2\theta}{\partial x^2} + \kappa_{16}\frac{\partial^2\theta}{\partial y^2} + \kappa_{17}\left(\frac{\partial\theta}{\partial x}\right)^2 + \kappa_{18}\left(\frac{\partial\theta}{\partial y}\right)^2 \end{aligned} \tag{14 c}$$

where the elastic functions $\{\kappa_i\}$, $i=1, \ldots, 18$, are given in the Appendix.

The dimensionless equations are obtained by scaling the temperature with T_{NI}, the elastic terms with K, the viscosity terms with γ_1, the distances x and y with R, and the time with $\gamma_1 R^2/K$. By doing this, the elastic functions become $\kappa_i^* = \kappa_i/K$. The superscript asterisk denotes a dimensionless variable. The equations then become the following set of dimensionless non-linear partial differential equations:

$$\frac{\partial T^*}{\partial t^*} = \alpha\left(\frac{\partial^2 T^*}{\partial x^{*2}} + \frac{\partial^2 T^*}{\partial y^{*2}}\right) \tag{15 a}$$

$$\begin{aligned} -\frac{\partial\theta}{\partial t^*} = {} & \kappa_1^*\left(\frac{\partial\theta}{\partial x^*} + \frac{\partial\theta}{\partial y^*}\right)\left(\frac{\partial S}{\partial x^*} + \frac{\partial S}{\partial y^*}\right) + \kappa_2^*\left(\frac{\partial^2\theta}{\partial x^{*2}} + \frac{\partial^2\theta}{\partial y^{*2}}\right) \\ & + \kappa_3^*\frac{\partial S}{\partial x^*}\frac{\partial S}{\partial y^*} + \kappa_4^*\left(\frac{\partial S}{\partial x^*}\right)^2 + \kappa_5^*\left(\frac{\partial S}{\partial y^*}\right)^2 \\ & + \kappa_6^*\frac{\partial^2 S}{\partial x^{*2}} + \kappa_7^*\frac{\partial^2 S}{\partial y^{*2}} + \kappa_8^*\left(\frac{\partial\theta}{\partial x^*} - \frac{\partial\theta}{\partial y^*}\right)\left(\frac{\partial S}{\partial x^*} - \frac{\partial S}{\partial y^*}\right) \end{aligned} \tag{15 b}$$

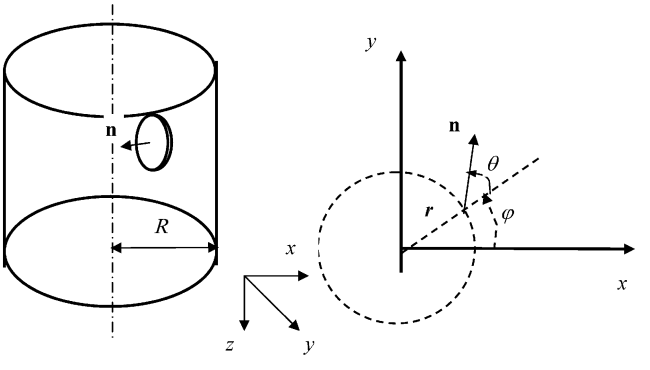

Figure 1. Schematic representation of the disc-like molecules within a section of a carbonaceous mesophase fibre of radius R, and the definition of the coordinate systems. The polar coordinates r–ϕ are expressed by dashed lines. The cartesian coordinates x–y are expressed by solid lines. θ is the planar director orientation angle measured in radians, which is the angle between director **n** and polar r at point (x, y).

$$-\frac{\partial S}{\partial t^*}=\beta\left[(T^*-1)S-S^2+2S^3\right](3+6S^2)+\kappa_9^*\left[\left(\frac{\partial\theta}{\partial x^*}\right)^2+\left(\frac{\partial\theta}{\partial y^*}\right)^2\right]+\kappa_{10}^*\left(\frac{\partial^2 S}{\partial x^{*2}}+\frac{\partial^2 S}{\partial y^{*2}}\right)+\kappa_{11}^*\frac{\partial\theta}{\partial x^*}\frac{\partial S}{\partial x^*}+\kappa_{12}^*\frac{\partial\theta}{\partial y^*}\frac{\partial S}{\partial y^*}+\kappa_{13}^*\frac{\partial^2 S}{\partial x^{*2}}+\kappa_{14}^*\frac{\partial^2 S}{\partial y^{*2}}+\kappa_{15}^*\frac{\partial^2\theta}{\partial x^{*2}}+\kappa_{16}^*\frac{\partial^2\theta}{\partial y^{*2}}+\kappa_{17}^*\left(\frac{\partial\theta}{\partial x^*}\right)^2+\kappa_{18}^*\left(\frac{\partial\theta}{\partial y^*}\right)^2. \quad (15\,c)$$

Equation (15) introduces a dimensionless thermal diffusivity α and a dimensionless characteristic molecular free energy β, which are expressed as follow:

$$\alpha=\frac{k_{\text{th}}}{\rho C_p}\frac{\gamma_1}{K} \quad (16)$$

and

$$\beta=\frac{k_{\text{B}}\upsilon T_{\text{NI}}R^2}{K}. \quad (17)$$

The dimensionless thermal diffusivity α depends on both the melt transport properties and the liquid crystalline properties. In this study, we use the range $1\leqslant\alpha\leqslant10^5$. β is defined as the ratio of short range order elasticity to long range order elasticity [20], and in this study we use $\beta=10^4$ to be consistent with prior published theoretical work [20]. Furthermore, these values allow us to fulfill the objectives listed in the introduction.

The material physical properties and the melt spinning process parameters used in this model are shown in tables 1 to 3. The values for K, K_5, and K_6 are obtained by assuming a ratio of L_2/L_1, which is in the same range as published theoretical work [20–23], since no experimentally determined values can be found for them. The absolute values of the three elastic constants are of the order of 10^{-12} N [24]. Furthermore, the elastic constants fulfill the constitutive hypothesis set by the following conditions [34]:

$$L_1\geq0 \text{ and } L_1+\frac{2}{3}L_2\geq0 \quad (18\,a,b)$$

Lastly, according to equations (6 b, c), $L_2<0$ is required for disc-like molecules.

The initial and boundary conditions are as follows:

$$T_i=T_S \text{ at } t=0,\ -R\leq x\leq R,\ -R\leq y\leq R \quad (19\,a)$$

$$\theta_i=\theta_{\text{o}}+\eta\varepsilon \text{ at } t=0,\ -R\leq x\leq R,\ -R\leq y\leq R \quad (19\,b)$$

$$S=0.25+0.75\left(1-\frac{8T_{\text{S}}}{9T_{\text{NI}}}\right)^{\frac{1}{2}} \text{ at } t=0,\ -R\leq x\leq R,\ -R\leq y\leq R \quad (19\,c)$$

$$T=T_{\text{C}} \text{ at } t>0,\ x^2+y^2=R^2 \quad (19\,d)$$

$$\theta=\theta_{\text{b}} \text{ at } t>0,\ x^2+y^2=R^2 \quad (19\,e)$$

$$S=0.25+0.75\left(1-\frac{8T_{\text{C}}}{9T_{\text{NI}}}\right)^{\frac{1}{2}} \text{ at } t>0,\ x^2+y^2=R^2 \quad (19\,f)$$

where T_S is the fibre spinning temperature, T_{C} is the cooling air temperature, and T_{NI} is the nematic–isotropic phase transition temperature. Values for these temperatures are listed in table 2.

The initial condition used in this paper attempts to mimic reality by including thermal fluctuations in the director orientation. This is done by equation (19 b), where θ_{o} is the average director orientation inherited from upstream. ε is a random number determined using a standard random number generator and is within the range $0<\varepsilon<1$, and η is a factor that controls the magnitude of the fluctuation. In this study, we use $\eta=0.5$. The choice of the algebraic operation $\pm$ is determined randomly by using a random number generator with a different seed than that used to generate ε. If the random number generated is less than 0.5, the sign is negative; otherwise, it is positive.

The realistic boundary conditions used in this study represent two typical surface anchoring behaviours of

Table 1. Elastic constants.

$K=9L_1+\frac{9}{2}L_2$	30.0×10^{-12} N
$K_5=\frac{3}{2}L_1+\frac{1}{4}L_2$	6.0×10^{-12} N
$K_6=\frac{3}{4}L_2$	-1.5×10^{-12} N

Table 2. Melt spinning parameters.

Parameter	Value/K	Ref.
T_{S} (fibre spinning temperature)	600	[1]
T_{C} (cooling air temperature)	373	[1]
T_{NI} (nematic–isotropic transition temperature)	725	[11]

Table 3. Physical properties for carbon fibres.

Property	Value	Ref.
R (fibre radius)	5.5×10^{-6} m	[1]
ρ (mesophase pitch density)	2000 kg m^{-3}	[1]
C_p (heat capacity)	1250 J kg^{-1} K^{-1}	[3]
k_{th} (thermal conductivity)	7.5 W m^{-1} K^{-1}	[4]

mesophase pitch molecules during the fabrication of carbon fibres. One boundary condition represents the case where the discotic liquid crystalline molecules are oriented with the aromatic rings perpendicular to the spinneret. This is obtained by setting the directors, which are perpendicular to the discotic molecules, at $\theta_b=0$. Another possible boundary condition for the director field is where the discotic liquid crystalline molecules are aligned parallel (i.e. tangential) to the spinneret surface. This is represented in the model by setting the director orientation angles at the spinneret surface to be 90°, i.e. $\theta_b=\pi/2$ radians. The director initial average angles and boundary orientations θ_o and θ_b used in the simulation for this paper are listed in table 4. These values enable us to achieve the objectives stated earlier.

In summary, the dependent variables are the dimensionless temperature T^*, the scalar order parameter S and director orientation θ. The independent variables are the dimensionless lengths x^* and y^*, and the dimensionless time t^*. Equations (15 *a–c*) are solved numerically with the dimensionless initial and boundary conditions given by equations (A3) in the Appendix. The Galerkin finite element method is used with 300 quadrilateral elements and isoparametric mapping. The time integrator is the first order Euler predicator–corrector method, and the Newton–Raphson method is used for solving the system of non-linear algebraic equations.

3. Results and discussion

This section presents and discusses representative numerical solutions to equations (15 *a–c*) and (A3 *a–f*). We begin by showing the time evolution of the molecular field resulting from computer simulation where $\alpha=10^3$ and $\beta=10^4$. Then the temperature and the scalar order parameter spatial profiles for $\alpha=10^3$ and $\beta=10^4$ are presented. This is followed by a discussion on the effect of the dimensionless thermal diffusivity α on the thermal relaxation phenomenon. We conclude this section with a discussion on how the dimensionless thermal diffusivity α affects the structure development and texture formation in carbon fibres.

Figure 2 shows the structure development and texture formation across the mesophase fibre when $\alpha=10^3$ and $\beta=10^4$ for case 1 (first column), and case 2 (second column) at the following dimensionless times t^*: (*a*) 0.0, (*b*) 0.01, (*c*) 0.016, and (*d*) 0.05. The short line segments represent the edges of the discotic molecules, and are obtained by noting that a director is normal to the disc-like molecule. The first column shows that, under the initial and boundary conditions restricted by case 1, the molecules go from a randomly aligned state to a quasi-onion state, and finally evolve into a perfectly concentric (i.e. onion) structure. In contrast, the second column shows that under the restrictions from case 2, the molecules start from a randomly aligned state to a zig-zagged radial texture, eventually evolving into a perfectly radial structure. The scientific visualizations of the fibre cross-sectional textures plotted from the computer simulations indicate that the mesophase pitch based carbon fibre texture formation is a combination of mode (radial or onion) selection and structure development. The mode selection between the radial and onion textures depends on the mesophase pitch textures inherited from the upstream processes and surface anchoring behaviours of mesophase pitch molecules. This is consistent with the experimental observations reported by Hamada *et al* [38]. They found that the transverse textures of mesophase fibre could be controlled by changing the pitch flow conditions at the upper portion of the spinneret during melt spinning. Wang and Rey [39] also predicated that fixed arbitrary surface orientation of mesophase pitch molecules affects the fibre textures. Lastly, figure 2 shows that the fibre textures evolve from stressed high energy states to structures with minimal distortion Frank elastic free energy at steady state.

Table 4. Auxiliary conditions.

	Angle/rad	
Orientation	Case 1	Case 2
Initial director average orientation, θ_o	$\theta_o=\frac{\pi}{2}$	$\theta_o=0$
Boundary director orientations, θ_b	$\theta_b=\frac{\pi}{2}$	$\theta_b=0$

Figure 3 is a plot of the stored dimensionless Frank elastic free energy F_d^* versus dimensionless time t^*. The two-dimensional dimensionless form of F_d^* may be obtained using equation (5) and is expressed as:

$$F_d^*=\frac{1}{4}\iint S^2\left(\frac{\partial\theta}{\partial x^*}+\frac{\partial\theta}{\partial y^*}\right)^2 dx\,dy. \qquad (20)$$

In order to characterize the time evolution of the molecular reorientation from the totally random oriented state to the well-defined structures at steady state, we define τ_d and τ_o as the time required for the molecules to reorient such that the Frank elastic free energy F_d^* decreases by 86.5% and 98%, respectively. For this case, $\tau_d=0.016$ and $\tau_o=0.05$. This figure shows that the Frank elastic free energy F_d^* evolution goes through three stages: fast, intermediate, and weak relaxation. The three relaxation stages are consistent with the texture development exhibited in figure 2. In the fast relaxation stage, corresponding to $t^*<0.016$ (or τ_d) in figure 2, the molecules are initially randomly

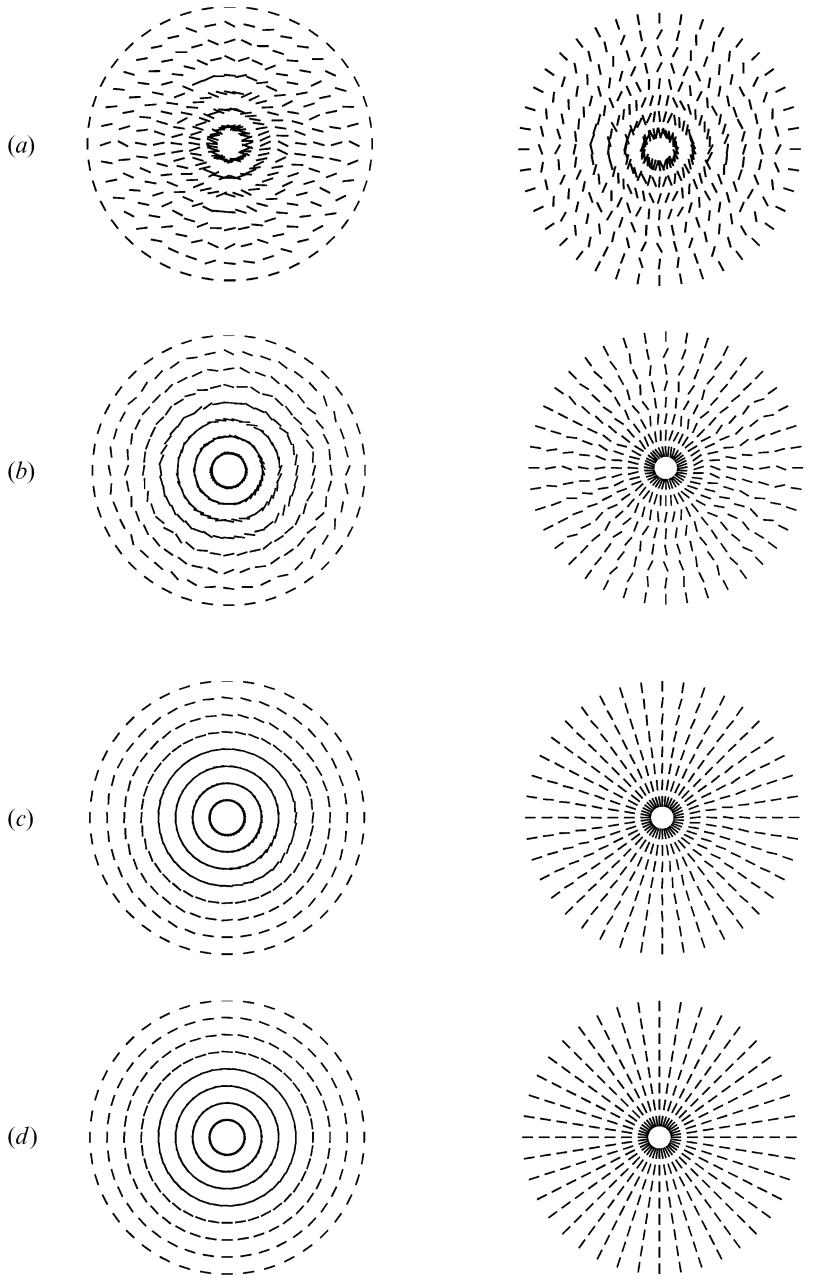

Figure 2. Typical relaxation phenomena for molecular orientation for the case $\alpha=10^3$ and $\beta=10^4$, across fibre transverse section at the following dimensionless times t^*: (*a*) 0.0, (*b*) 0.01, (*c*) 0.016 and (*d*) 0.05.

oriented which leads to a strained texture. This initial texture stores the greatest-level distortion free energy, which is the driving force for the fast relaxation rate for $t^*<\tau_d$. In stage 2, corresponding to 0.016 (or τ_d)$<t^*<$0.05 (or τ_o) in figure 2, the Frank free energy F_d^* decreases from 13.5% to 2% of its initial value; the molecules form well defined structures at the end of this time period. In the final weak relaxation stage, corresponding to $t^*>$0.05 (or τ_o) in figure 2, the residue of the Frank elastic free energy F_d^* is the small driving force to reorient the molecules into the onion or radial textures. In summary, the director relaxation phenomena can be well explained using the Frank elastic free energy theory. Discotic nematics are elastic materials, where energy is stored by orientational strains. The driving force for the texture development from a

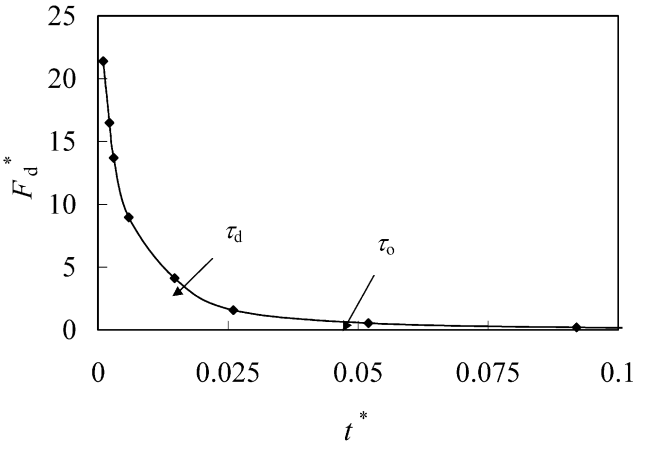

Figure 3. Time evolution of the dimensionless Frank elastic free energy F_d^* for the case $\alpha=10^3$ and $\beta=10^4$. τ_d and τ_o are defined as the time required for the molecules to reorient such that the Frank elastic free energy F_d^* decreases by 86.5% and 98%, respectively.

randomly aligned texture to well defined textures (such as the radial and onion textures) is the minimization of the stored Frank elastic free energy.

Figure 4 shows the two-dimensional relaxation phenomena of the temperature profile for the case when $\alpha=10^3$ and $\beta=10^4$ at the following dimensionless times t^*: (*a*) 0.02, (*b*) 0.03, (*c*) 0.04, and (*d*) 0.32. Figure 4 shows typical thermal diffusion phenomena along the fibre radial direction. The fibre exits the spinneret at spinning temperature $T_S=600\,K$, and is suddenly exposed to cooling air temperature at $T_C=373\,K$. It is assumed that there is perfect thermal contact between the cooling air and the mesophase pitch. As expected, the two-dimensional temperature spatial profile becomes uniform at long times (i.e. steady state). Figure 5 shows the two-dimensional relaxation phenomena of the scalar order parameter S for the case when $\alpha=10^3$ and $\beta=10^4$ at the following dimensionless times t^*: (*a*) 0.02, (*b*) 0.03, (*c*) 0.04, and (*d*) 0.32. It shows that the scalar order parameter S evolution is

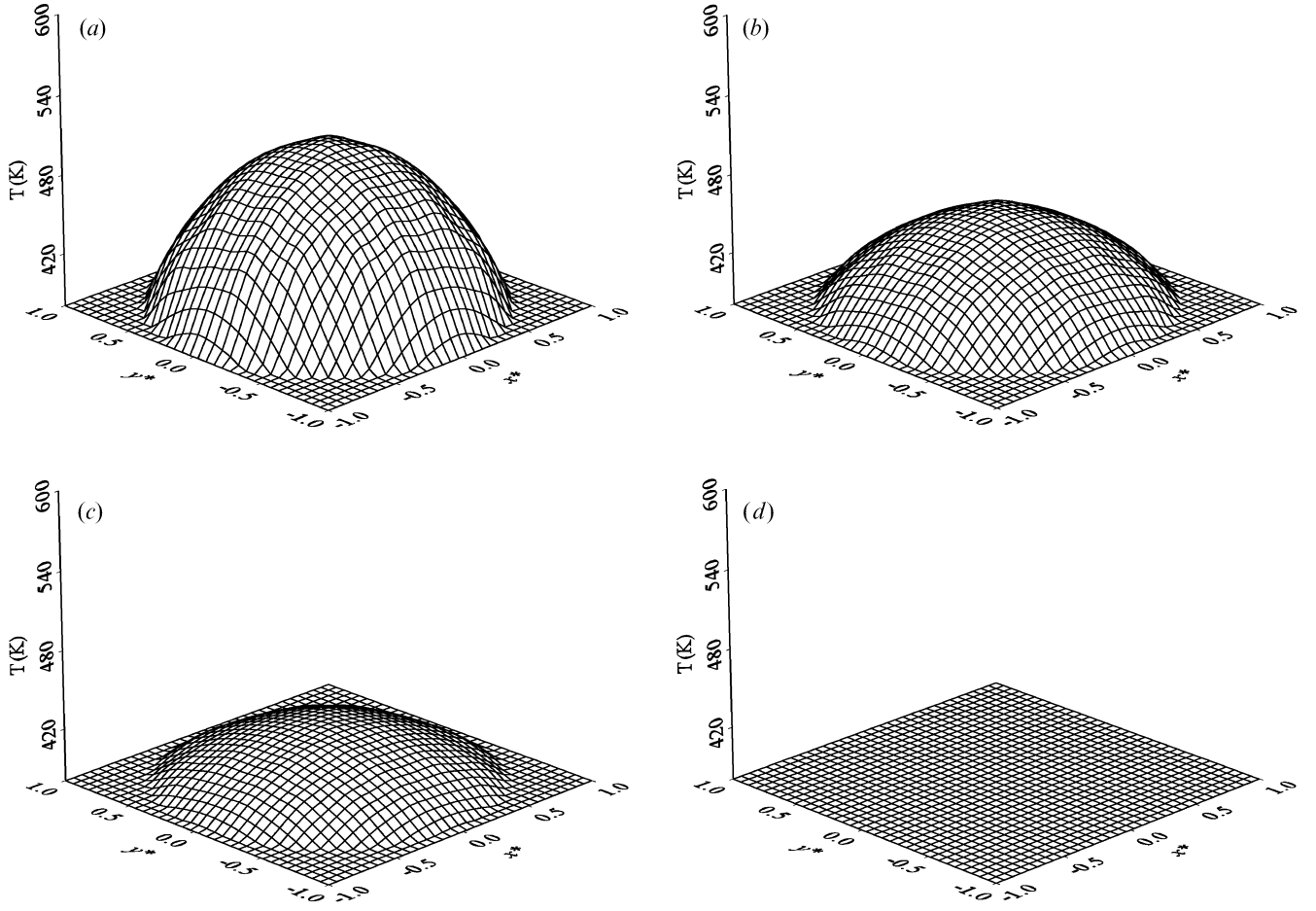

Figure 4. Typical relaxation phenomena of the temperature profile for the case $\alpha=10^3$ and $\beta=10^4$ at the following dimensionless times t^*: (*a*) 0.02, (*b*) 0.03, (*c*) 0.04 and (*d*) 0.32.

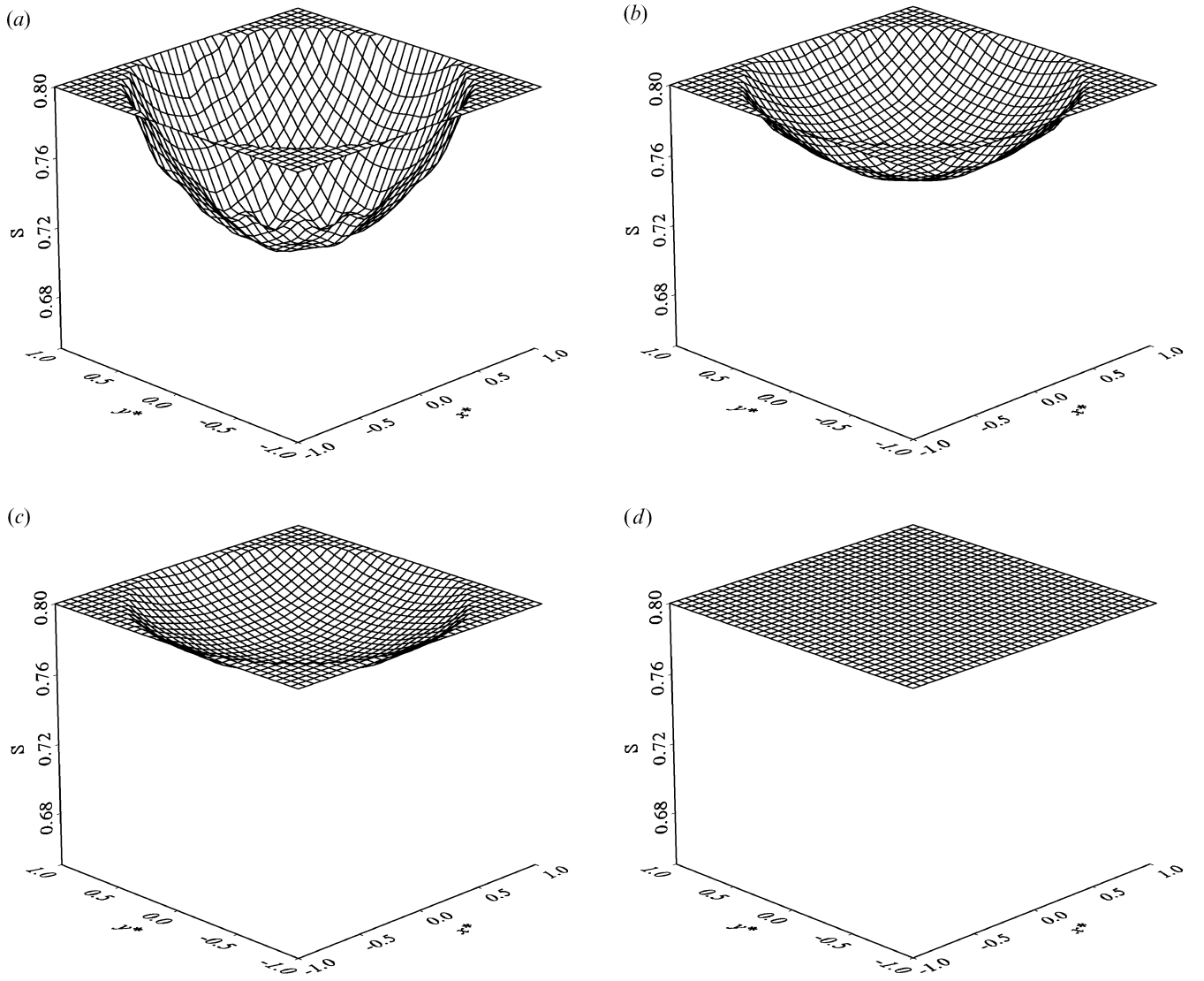

Figure 5. Typical relaxation phenomena of the scalar order parameter profile for the case $\alpha=10^3$ and $\beta=10^4$ at the following dimensionless times t^*: (*a*) 0.02, (*b*) 0.03, (*c*) 0.04 and (*d*) 0.32.

consistent with that of the temperature profile. This may be explained using the following temperature dependency of the scalar order parameter at homogeneous equilibrium [34]:

$$S_{eq}=0.25+0.75\left(1-\frac{8}{3U}\right)^{\frac{1}{2}} \qquad (21)$$

where $U=3T_{NI}/T$. For an isotropic phase $U<8/3$, while for a nematic phase $U>3$ [35]. For this model, nematic potential $U=3T_{NI}/T$ is inhomogeneous due to the temperature gradient across the fibre radius. The scalar order parameter S decreases as temperature increases and reaches steady state simultaneously with the temperature profile.

Figure 6 is a plot of the time evolution of the molecular free energy F_S^* for the case when $\alpha=10^3$ and $\beta=10^4$, which was calculated by integrating equation (7) over the fibre cross-section area. Figure 6 indicates that F_S^* decreases with time, and reaches steady state at the same time as the spatial profiles of temperature and the scalar order parameter (see figures 4 and 5). The time when F_S^* decreases to the steady state value is denoted as the thermal relaxation process steady state time τ_α. For this case, the plot shows $\tau_\alpha=0.32$, and is consistent with the time required for temperature T and the scalar order parameter S to reach steady state in figures 4 and 5.

Figure 7 is a plot of the dimensionless times τ_d, τ_o and τ_α versus thermal diffusivity α. This figure is used to display the effect of the dimensionless thermal

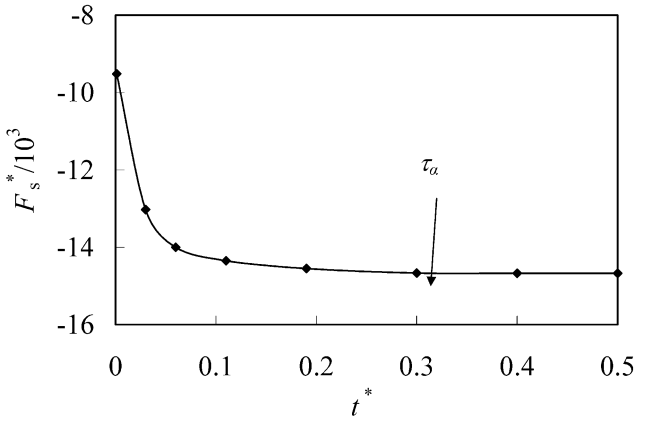

Figure 6. Time evolution of the dimensionless molecular free energy F_S^* for the case $\alpha=10^3$ and $\beta=10^4$. τ_α is the time for the molecular free energy to reach steady state.

diffusivity α on mesophase pitch-based carbon fibre texture formation and structure development. The slanted dashed line indicates that the thermal relaxation steady state time τ_α decreases monotonically with dimensionless thermal diffusivity α. This means that the time for S and T to reach steady state decreases as α increases. The reason for this phenomenon is that the dimensionless thermal diffusivity is the factor that controls the rate of heat transfer between the mesophase pitch and the cooling air, see equation (9), i.e. the rate of heat transfer increases with α. The two solid near-horizontal lines represent the dependences of the dimensionless director reorientation times τ_o and τ_d versus the dimensionless thermal diffusivity α. The nearly flat lines show that the dimensionless thermal

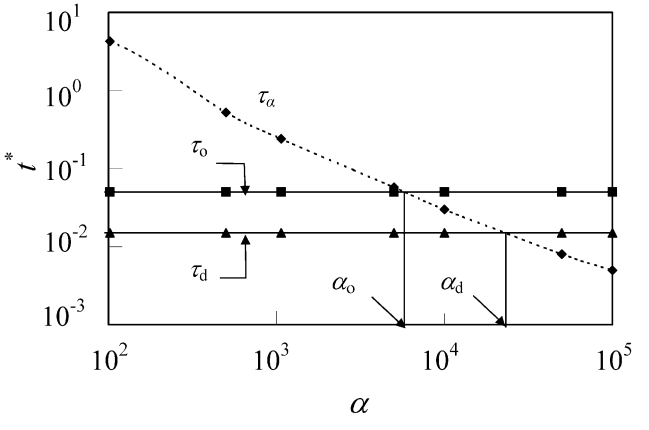

Figure 7. The effect of the thermal diffusivity α on the thermal relaxation. The dashed line represents the thermal relaxation time scale versus α. The two solid lines represent the molecule reorientation time scales versus α. α_o is defined as the cross point between τ_o and τ_α, and α_d is the cross point between τ_d and τ_α.

diffusivity α has little effect on the director field relaxation. The reason for this fact is that the relaxation rate of f_d^* is a function of elastic constants and not a function of α. The dynamic behaviour of the director reorientation is governed by equation (15 *b*) where the right hand side has eight terms. The first term, the second term and the last six terms are obtained, respectively, from f_e^*, f_d^* and f_C^*. The simulation results indicated that, compared with Frank elastic free energy, f_e^* and f_C^* induced by interaction between S and **n** spatial gradients are negligible. Therefore, the effect of the first term and the last six terms on the director reorientation in equation (15 *b*) can be neglected. Consequently, the time evolution of the director field in the two-dimensional study can be expressed as:

$$-\frac{\partial\theta}{\partial t^*}=\kappa_2^*\left(\frac{\partial^2\theta}{\partial x^{*2}}+\frac{\partial^2\theta}{\partial y^{*2}}\right). \tag{22}$$

Equation (22) shows that the relaxation of director field is not affected by the thermal diffusivity because the dimensionless elastic function κ_2^* is related only to Landau elastic constants, see equation (A2 b). The other seven terms of equation (15 *b*) have little effect on the director evolution. This leads to the director reorientation behaviour being nearly independent of the scalar order parameter S and temperature T fields.

To characterize the thermal diffusivity effect on the structure development and texture formation, we define α_o as the value of α at the cross-over point between τ_α and τ_o; the value at the cross-over point between τ_α and τ_d is denoted as α_d. As discussed above, τ_α may be taken as the time for the temperature T and the scalar order parameter profile S spatial profiles to reach steady state. Furthermore, τ_o and τ_d may be taken as the time for the liquid crystal molecule spatial profile to reorient to within 13.5% and 2%, respectively, of its steady state profile. High value of α indicates higher viscosity, lower elasticity and a fast cooling rate; low value of α represents lower viscosity, higher elasticity and a slow cooling process.

For $\alpha>\alpha_d$, the plot shows process time τ_α is less than reorientation times τ_d and τ_o. This means there is little time available for discotic molecules to rotate. This leads to a partially aligned texture depicted in figure 2 (*b*). For $\alpha_o<\alpha<\alpha_d$, figure 6 indicates $\tau_d<\tau_\alpha<\tau_o$. When α is between these values, the molecules will have more time to reorient into the well developed textures (i.e. radial and onion textures), which are exhibited in figure 2 (*c*). For $\alpha<\alpha_o$, the plot shows $\tau_\alpha>\tau_d$ and τ_o. This means the reorientation time provided by the thermal relaxation process for molecules to rotate is longer than the time that the molecules require to reorient to well

developed radial or onion textures as shown in figure 2 (*d*).

4. Conclusion

The Ericksen and Landau–de Gennes continuum theories were used in this paper to study numerically the structure development and texture formation in a discotic uniaxial nematic mesophase pitch-based carbon fibre after cessation of extensional flow. The selection between the radial and onion textures depends on the surface orientation angle in the mesophase pitch upon exiting the spinneret. Moreover, the resulting texture depends on the times required for director reorientation and heat transfer. The structure development is affected by the cooling rate, pitch melt viscosity and elasticity. High thermal diffusivity caused by higher viscosity and fast cooling inhibits the liquid crystal molecular reorientation and limits the structure development. Lower viscosity and slow cooling provide more time for liquid crystal molecular reorientation and allow fibre cross-sectional structure to develop into well defined textures. These simulation results provide additional information on molecular orientation during post melt spinning process, which helps to improve the product properties and to reduce the post treatment process cost.

Acknowledgements

The authors gratefully acknowledge the financial support from Ryerson University and the Natural Sciences and Engineering Research Council of Canada (NSERC).

References

[1] L.H. Peebles. *Carbon Fibres Formation, Structure, and Properties*. CRC Press, London (1995).
[2] D.D. Edie. *Carbon*, **36**, 345 (1998).
[3] D.D. Edie, M.G. Dunham. *Carbon*, **27**, 647 (1989).
[4] J.B. Donnet, R. Bansal. *Carbon Fibres*. Marcel Dekker, New York (1990).
[5] K.E. Robinson, D.D. Edie. *Carbon*, **34**, 13 (1996).
[6] J.J. McHugh, D.D. Edie. *Carbon*, **34**, 1315 (1996).
[7] I. Mochida, S.H. Yoon, N. Takano. *Carbon*, **34**, 941 (1996).
[8] N.C. Gallego, D.D. Edie. *Carbon*, **38**, 1003 (2000).
[9] I. Mochida. *Carbon*, **38**, 305 (2000).
[10] J.D. Fitz, G.M. Pennock, G.H. Taylor. *Carbon*, **29**, 1139 (1991).
[11] M. Shishido, H. Inomata, K. Arai, S. Saito. *Carbon*, **35**, 797 (1997).
[12] G. Lubin. *Handbook of Composites*. Van Nostrand Reinhold Company, New York (1981).
[13] M. Matsumoto, T. Iwashita, Y. Arai, T. Tomioka. *Carbon*, **31**, 715 (1993).
[14] J.J. McHugh, D.D. Edie. *Liq. Cryst.*, **18**, 327 (1995).
[15] K.E. Roberson, D.D. Edie. *Carbon*, **34**, 13 (1996).
[16] A.P. Singh, A.D. Rey. *Liq. Cryst.*, **26**, 825 (1999).
[17] A.P. Singh, A.D. Rey. *Rheol. Acta*, **37**, 30 (1998).
[18] A.P. Singh, A.D. Rey. *Rheol. Acta*, **37**, 374 (1998).
[19] A.P. Singh, A.D. Rey. *Liq. Cryst.*, **18**, 219 (1995).
[20] A.P. Singh, A.D. Rey. *J. non-Newtonian fluid Mech.*, **94**, 87 (2000).
[21] J. Yan, A.D. Rey. *Carbon*, **41**, 105 (2003).
[22] D. Sharma, A.D. Rey. *Liq. Cryst.*, **30**, 377 (2003).
[23] J. Yan, A.D. Rey. *Carbon*, **40**, 2647 (2002).
[24] P.G. de Gennes, J. Prost. *The Physics of Liquid Crystals*. Clarendon Press, Oxford (1974).
[25] P. Sheng, E.B. Prestley, P.J. Wojtowicz. *Introduction to Liquid Crystals*. Plenum Press, New York (1974).
[26] I.-C. Khoo, F. Simoni. *Physics of Liquid Crystalline Materials*. Gordon and Breach, New York (1991).
[27] S. Chandrasekhar. *Liquid Crystals.* 2nd Edn, Cambridge University Press, Cambridge (1992).
[28] W.H. de Jeu. *Thermotropic Liquid Crystals: Fundamentals*. Springer-Verlag, New York (1988).
[29] W.H. de Jeu. *Physical Properties of Liquid Crystalline Materials*. Gordon and Breach, New York (1980).
[30] L. Wang, A.D. Rey. *Modeling Simulation in Material Science Engineering.* Vol. 5, pp. 67–77 (1997).
[31] J.L. White, M. Buchler. In *Petroleum-Derived Carbons*, J.D. Bacha, J.W. Newman, J.L. White (Eds), pp. 62–84, ACS., Washington (1986).
[32] J.L. Ericksen. IMA Reprint Series, No. 559 (1989).
[33] P.K. Chan, A.D. Rey. *Liq. Cryst.*, **13**, 775 (1993).
[34] A.N. Beris, B.J. Edwards. *Thermodynamics of Flowing Systems*. Clarendon, Oxford (1994).
[35] M. Doi, B.J. Edwards. *The Theory of Polymer Dynamics*. Clarendon, Oxford (1986).
[36] R.B. Bird, W.E. Stewart, E.N. Lightfoot. *Transport Phenomena*. Wiley, New York (1960).
[37] O. Parodi. *J. Phys.*, **31**, 581 (1970).
[38] T. Hamada, T. Nishada, M. Furuyama, T. Tomioka. *Carbon*, **26**, 837 (1988).
[39] L. Wang, A.D. Rey. *Liq. Cryst.*, **23**, 93 (1997).

Appendix

The relationships for the dependency of the Leslie viscosities on the scalar order parameter S are as follows [34]:

$$\alpha_1^S = \beta_1^m S^2 - \frac{\left(\gamma_2^S\right)^2}{\gamma_1^S} + \frac{\left(\beta_1^S\right)^2}{\beta_2^S} \qquad \text{(A1 } a\text{)}$$

$$\alpha_2^S = \frac{1}{2}\left(\gamma_2^S - \gamma_1^S\right) \qquad \text{(A1 } b\text{)}$$

$$\alpha_3^S = \frac{1}{2}\left(\gamma_2^S + \gamma_1^S\right) \qquad \text{(A1 } c\text{)}$$

$$\alpha_4^S = \beta_4^m + \frac{2}{3}\beta_2^S(1-S) + \frac{2}{9}\beta_3^m(1-S)^2 + \frac{1}{9}\beta_1^m(1-S)^2 \qquad \text{(A1 } d\text{)}$$

$$\alpha_5^S = \frac{1}{3}\beta_1^m S(1-S) + \beta_2^m S + \alpha_2^S \frac{\gamma_2^S}{\gamma_1^S} \quad \text{(A1 } e\text{)}$$

$$\alpha_6^S = \gamma_2^S + \alpha_5^S \quad \text{(A1 } f\text{)}$$

$$\beta_1^S = \beta_2^S \frac{\alpha_3+\alpha_2}{\alpha_3-\alpha_2}(2S+1)(1-S) \quad \text{(A1 } g\text{)}$$

$$\beta_2^S = \frac{\alpha_3-\alpha_2}{3+6S^2} \quad \text{(A1 } h\text{)}$$

$$\gamma_1^S = S^2(\alpha_3-\alpha_2) \quad \text{(A1 } i\text{)}$$

$$\gamma_2^S = \gamma_1^S \frac{(\alpha_3+\alpha_2)}{(\alpha_3-\alpha_2)} \frac{2+S}{3S} \quad \text{(A1 } j\text{)}$$

$$\beta_1^m = \alpha_1+\alpha_2-\alpha_3+4\frac{\alpha_2\alpha_3}{\alpha_2-\alpha_3} \quad \text{(A1 } k\text{)}$$

$$\beta_2^m = \frac{1}{2}\alpha_2 \quad \text{(A1 } l\text{)}$$

$$\beta_3^m = \frac{1}{2}(\alpha_2+\alpha_5)+2\frac{\alpha_2\alpha_3}{\alpha_2-\alpha_3} \quad \text{(A1 } m\text{)}$$

$$\beta_4^m = \alpha_4. \quad \text{(A1 } n\text{)}$$

The elastic functions $\{\kappa_i\}$, $i=1, \ldots, 18$, in equations (14 *b*, *c*) are defined as follows:

$$\kappa_1 = -\frac{K}{S} \quad \text{(A2 } a\text{)}$$

$$\kappa_2 = -\frac{1}{2}K \quad \text{(A2 } b\text{)}$$

$$\kappa_3 = \frac{1}{S^2}K_6 \cos(2\theta) \quad \text{(A2 } c\text{)}$$

$$\kappa_4 = -\frac{1}{S^2}K_6(1+\cos^2\theta) \quad \text{(A2 } d\text{)}$$

$$\kappa_5 = \frac{1}{S^2}K_6(1+\sin^2\theta) \quad \text{(A2 } e\text{)}$$

$$\kappa_6 = -\frac{1}{S}K_6(1+\cos^2\theta-\sin\theta\cos\theta) \quad \text{(A2 } f\text{)}$$

$$\kappa_7 = \frac{1}{S}K_6(1+\sin^2\theta-\sin\theta\cos\theta) \quad \text{(A2 } g\text{)}$$

$$\kappa_8 = \frac{1}{S}K_6 \sin(2\theta) \quad \text{(A2 } h\text{)}$$

$$\kappa_9 = \frac{1}{2}KS(3+6S^2) \quad \text{(A2 } i\text{)}$$

$$\kappa_{10} = -K_5(3+6S^2) \quad \text{(A2 } j\text{)}$$

$$\kappa_{11} = 3K_6(3+6S^2)(\sin\theta\cos\theta+\sin^2\theta) \quad \text{(A2 } k\text{)}$$

$$\kappa_{12} = -3K_6(3+6S^2)(\sin\theta\cos\theta+\cos^2\theta) \quad \text{(A2 } l\text{)}$$

$$\kappa_{13} = -K_6(3+6S^2)(\sin\theta\cos\theta+\cos^2\theta) \quad \text{(A2 } m\text{)}$$

$$\kappa_{14} = -K_6(3+6S^2)(\sin\theta\cos\theta+\sin^2\theta) \quad \text{(A2 } n\text{)}$$

$$\kappa_{15} = K_6S(3+6S^2)(1+\sin\theta\cos\theta+\sin^2\theta) \quad \text{(A2 } o\text{)}$$

$$\kappa_{16} = -K_6S(3+6S^2)(1+\sin\theta\cos\theta+\cos^2\theta) \quad \text{(A2 } p\text{)}$$

$$\kappa_{17} = K_6S(3+6S^2)[\sin(2\theta)+\cos(2\theta)] \quad \text{(A2 } q\text{)}$$

$$\kappa_{18} = K_6S(3+6S^2)[\sin(2\theta)-\cos(2\theta)] \quad \text{(A2 } r\text{)}$$

where the following relations between elastic constants K, K_5 and K_6 and Landau coefficients have been used:

$$K = 9L_1+\frac{9}{2}L_2 \quad \text{(A2 } s\text{)}$$

$$K_5 = \frac{3}{2}L_1+\frac{1}{4}L_2 \quad \text{(A2 } t\text{)}$$

$$K_6 = \frac{3}{4}L_2. \quad \text{(A2 } u\text{)}$$

The dimensionless initial and boundary conditions are as follows:

$$T_i^* = T_S/T_{NI} \text{ at } t^*=0,\ -1\le x^*\le 1,\ -1\le y^*\le 1 \quad \text{(A3 } a\text{)}$$

$$\theta_i = \theta_0+\eta\varepsilon \text{ at } t^*=0,\ -1\le x^*\le 1,\ -1\le y^*\le 1 \quad \text{(A3 } b\text{)}$$

$$S = 0.25+0.75\left(1-\frac{8T_S}{9T_{NI}}\right)^{\frac{1}{2}} \quad \text{(A3 } c\text{)}$$
$$\text{at } t^*=0,\ -1\le x^*\le 1,\ -1\le y^*\le 1$$

$$T^* = T_C/T_{NI} \text{ at } t^*>0,\ x^{*^2}+y^{*^2}=1 \quad \text{(A3 } d\text{)}$$

$$\theta = \theta_b \text{ at } t^*>0,\ x^{*^2}+y^{*^2}=1 \quad \text{(A3 } e\text{)}$$

$$S = 0.25+0.75\left(1-\frac{8T}{9T_{NI}}\right)^{\frac{1}{2}} \text{ at } t^*>0,\ x^{*^2}+y^{*^2}=1. \quad \text{(A3 } f\text{)}$$